Space-Enhanced Terrestrial Solar Power for Equatorial Regions [a]

F. Bonetti[b] and C. McInnes[c]
School of Engineering, University of Glasgow, Glasgow, G12 8QQ

This paper investigates the concept of solar mirrors in a Earth orbit to provide large-scale terrestrial equatorial solar farms with additional solar power during the hours of darkness. A flower constellation of mirrors is considered in highly-eccentric orbits (semi-major axis=20270.4 km) in order to increase the time of visibility over the solar farms and, through this architecture, only two mirrors are needed to provide a complete night-coverage over three equatorial locations. Selecting the proper value for the orbit eccentricity, solar radiation pressure and Earth's oblateness perturbations act on the mirrors so that the apsidal motion of the orbit due to these perturbations is synchronized with the apparent motion of the Sun. Therefore, it can be guaranteed that the perigee always points towards the Sun and that the mirrors orbit mostly above the night side of the Earth. With respect to Geostationary orbit (GEO), the family of orbits considered in this paper allow a passive means to overcome issues related to orbital perturbations. Moreover, because of the large slant range from GEOs, a larger mirror is required to deliver the same energy that could be delivered from a lower orbit with a smaller mirror. As a result, a single anti-heliotropic flower constellation comprised of two mirrors of 50 km^2 would be able to deliver energy in the range of $4.60 - 5.20$ GWh per day to 1000 km^2-solar farms on the equator. Finally, it is estimated that, deploying 90 of these constellations, the price of electricity could be reduced from 9.1 cents to 6 cents per kWh.

[a] previously presented at the 27^{th} AAS/AIAA Space Flight Mechanics Meeting, San Antonio, Texas, 2017.
[b] PhD candidate, Department of Systems Power and Energy, F.Bonetti.1@research.gla.ac.uk
[c] Professor of Engineering Science, Department of Systems Power and Energy, Colin.McInnes@glasgow.ac.uk

Nomenclature

α	incidence angle for the first steering law	rad
α'	incidence angle for the second steering law	rad
β	angle subtended by the Sun	rad
γ	half umbral cone apex	rad
δ	vector originating at the umbral cone axis pointing to the spacecraft	m
ϵ	elevation angle	rad
ϵ_{GCR}	losses due to the ground coverage ratio	
ϵ_{PV}	losses due to the solar farm photovoltaic array modules	
ζ	Earth central angle	rad
η	nadir angle	rad
λ	longitude of the solar farm	rad
$\dot{\lambda_s}$	Sun's angular velocity in the Earth's central inertial frame	rad/s
μ	standard gravitational parameter of the Earth	m^3/s^2
ξ	distance between the umbral cone axis and the umbra terminator point	m
ρ	Earth angular radius	rad
σ	root-mean-square edge gradient of the membrane	rad
σ_s	sail loading	kg/m^2
τ	atmospheric trasmissivity	
ϕ	latitude of the solar farm	rad
χ_u	distance between the umbral cone apex and the centre of the Earth	m
ψ	cloud cover coefficient	
Ω	right ascension of the ascending node	rad
ω	argument of perigee	rad
ω_e	Earth angular velocity	rad/s
$\hat{s}$	unit vector indicating the Sun's direction	

A	area	m^2
a	semi-major axis	m
a_{J_2}	acceleration due to J_2 perturbation	m/s^2
a_{SRP}	acceleration due to solar radiation pressure	m/s^2
C_r	reflectivity coefficient	
D	diameter	m
d_{im}	linear dispersion of the image,	m
e	eccentricity	
E_{SF}	total energy produced by each solar farm per day	Wh
f	true anomaly	rad
f_c	flatness coefficient	
i	inclination	rad
I_0	solar constant	W/m^2
J_2	Earth oblateness	
M	mean anomaly	rad
m	mass of the reflector	kg
N_d	number of days	
N_p	number of petals	
N_s	number of satellites	
p	semilatus rectum	m
P_M	power delivered by the mirror	W
P_{SF}	total power provided to the solar farm	W
P_{SRP}	solar pressure at 1 AU	N/m^2
R	radial component of the acceleration due to perturbations	m/s^2
r	position vector of the reflector in the Earth's central inertial frame	m
R_E	Earth radius	m
r_s	projection over the Sun-Earth line of the position vector of the reflector	m
r_{sp}	reflectivity of the material	
T	transversal component of the acceleration due to perturbations	m/s^2

T_a	anomalistic period	s
T_G	Greenwich nodal period	s
T_r	period of repetition	s
y	slant range	m

Subscripts

day	overall variation over 1 day
ECL	orbit of the reflector during which the eclipse takes place
$ecl1,2$	beginning and end of the eclipse
i	illuminated spot on the ground without spill-over area
if	image produced by a flat mirror
ip	image produced by a parabolic mirror
$itot$	overall illuminated area on the ground
M	mirror
max	maximum value allowed
min	minimum value allowed
R	radial component
SF	solar farm
$SF1,2,3$	first, second and third solar farm
$SRP = 0$	perturbations of solar radiation pressure are zero
T	transversal component

I. Introduction

This paper discusses the use of orbiting mirrors to improve the efficiency of large-scale terrestrial solar power farms. Placing mirrors in space, in a convenient orbit around the Earth, would make it possible to reflect sunlight downwards illuminating solar farms during the night. The reflected sunlight therefore needs to point towards a specific location on the ground where a series of large collectors will benefit from this surplus energy for terrestrial use. It is estimated that the use of space mirrors in polar orbit for terrestrial solar power generation could potentially reduce the cost of solar electric power to less than 6 cents per kWh [1].

Initial ideas on the prospect of beaming sunlight from space towards the Earth were proposed in 1912, when K. Tsiolkovsky suggested that "rocketry would enable the collection in space of solar energy in amounts billions of times greater than available on Earth" [2] and in 1926 in "Plan of Space Exploration" [3], which consists of 16 steps designed to bring humans into space, includes the use of "solar radiation to grow food, to heat space quarters, and for transport throughout the solar system".

Afterwards, in 1978 Ehricke describes in [4] the project Power Soletta, entailed a constellations of 3 mirror-satellites in an circular Earth orbit at 4200 km altitude. However, because of the choice of the circular orbit, in order to reproduce normal daylight solar intensity (brightness equal to 1 solar constant) each mirror would have an area of 4617 km^2. We note that given a solar flux of 1362 W/m^2, a thin-film mirror with a areal density of order 10 g/m^2 delivers a huge power density of 130 kW/kg.

The choice of the reflector orbit is critical to determine the time of the day when the additional energy is provided and the duration of the contact with the solar farm. For example, interesting strategies would be to reflect sunlight in the evening and early morning hours [5] or, in general, during the night or at least during peak hours (evening).

Therefore, previous concepts consider polar Sun-synchronous orbits so that the mirror would never be in eclipse [5, 6]. However, in this case, the maximum time in view of the ground site is as low as 9 minutes, or, at most, 20 minutes if the solar mirror is able to steer, changing its attitude, in order to track the solar farm while it is visible. For this reason, more complex designs have been considered, for example, a constellations of 18 satellites is designed in [5]. Since it is not possible to have continuous access to a single location, these satellites would serve 40 evenly distributed terrestrial solar farms. However, in this paper, although space mirrors of 78 km^2 are considered in orbits of 1000 km, issues related to atmospheric drag and perturbations due to solar radiation pressure (SRP) are not addressed.

Low latitude locations with relatively low cloud coverage are arguably more suitable for this strategy. For this reason, the equatorial regions are the most appealing and, even if Sun-synchronous polar orbits would allow continuous reflection of sunlight, it is rather straightforward to note that

polar orbits would not be the most immediate choice for low latitude sites.

Other architectures regard the use space mirrors in Geosynchronous Equatorial orbits (GEOs), for example in [7] a fleet of satellites is considered in GEO to receive energy and to transmit a power beam to a station on the Earth's surface. Although the use of GEOs would allow for extended visibility of the Sun and the solar farms on the ground, electric propulsion is required for station keeping maneuvers in order to counteract SRP and J_2 perturbations. Moreover, for the purpose of reflecting sunlight onto the Earth's surface, because of the large slant range (distance between the mirror and solar farm) a larger mirror is required to deliver the same energy that would be delivered from a lower orbit, such as MEO (medium Earth orbit), with a smaller mirror.

Another family of orbits, heliotropic orbits, can also be considered for this purpose. As described in [8], heliotropic orbits are eccentric high-altitude families of Sun-synchronous orbits where the apogee or the perigee is forced to follow the Sun. In this specific case, the eccentricity of the orbits is chosen so that J_2 Earth oblateness and SRP perturbations (including changes in SRP due to the steering of the mirror) are balanced to generate quasi-frozen orbits able to track the Sun. These orbits present an interesting option for space solar power, where their analytical description has been detailed in [9]. In particular, the contribution of each source of the perturbations in terms of the percentage of the apsidal rotation is 99.9 % for SRP and 0.01 % for J_2. In this paper, taking into account the concept of heliotropic orbits, highly-eccentric equatorial orbits able to track the Sun will be considered to increase the time in view of the space mirror and to deal with SRP and J_2 perturbations. Specifically, so-called anti-heliotropic orbits, where the orbit apogee is in general directed away from the Sun, are employed.

Moreover, the steering law for the solar mirror to track the solar farm on the ground, while it is visible, will generates oscillations on the SRP perturbation. For this reason, the family of frozen orbits investigated in this paper will differ slightly from those found in prior work [9].

The goal of this specific paper is to provide a daily surplus of solar energy for at least 3 locations situated near the equator. Therefore, a key issue is to generate an orbit with a repeat ground track. This subject has been extensively investigated in the past and most orbital constellations have been developed around this requirement. For example, in 1981, the San Marco Project conceptualized

the "Sistema Quadrifoglio" as an equatorial constellation of four satellites [10]. In this concept, each satellite spends about 6 hours near the orbit apogee and two hours in transition between successive apogees. Due to the phasing of satellites in their orbits, 3 of the satellites are always near apogee and the other is in transition to replace the spacecraft with the largest mean anomaly. The three spacecraft near apogee (about 120° apart) have line-of-sight visibility of each other and each can observe well over 1/3 of the Earth's surface. This new way of designing satellite constellations has stimulated interesting concepts such as the "shape-preserving" constellation. The "Sistema Quadrifoglio" generated the basis of Flower Constellations, which can be set so that each satellite of the constellation has identical repeat ground tracks [10]. In this paper a flower constellation of two mirror-satellites (technically an "incomplete" flower constellation) has been designed to accomplish the goal of providing surplus solar energy to 3 large solar farms in Central Africa, the Pacific coast and Oceania.

All details of the orbits designed for the mirrors can be found in Tab. (1). In Sec. (II), the

Table 1: Summary of the orbital parameters employed for the orbits of the nigh mirrors following the second steering law (see Sec.II D) and other key information.

Mirror	**1**	**2**
type of orbit	antiheliotropic	antiheliotropic
A/m	50 m^2/kg	50 m^2/kg
semi-major axis	20270.4 km	20270.4 km
eccentricity	0.636	0.636
orbital period	8 h	8 h
inclination	$\simeq 0$	$\simeq 0$
Ω	0°	270°
M	0°	270°
ω	270°	270°
eclipse duration	20 min	58 min
slant range variation	$7439 - 33200$ km	$7439 - 33200$ km

Perturbation of the line of apsides is due to 99.9 % SRP and 0.01 % J_2 for both mirrors.

design of the mirror orbit is described in detail. In particular, in Sec. (II A), the most suitable flower constellation is considered and the required orbit semi-major axis is estimated. In Sec. (II B), the process used to evaluate the correct value for the orbit eccentricity is reported. The "anti-heliotropic" condition is then achieved exploiting SRP and J_2 perturbations also taking into account the eclipse duration. In the following subsections two steering laws are considered for the space mirror: the first entails the mirror always pointing at the centre of the Earth (Sec. (II C)), whereas according to the second steering law the exact position of the solar farm is tracked while the mirrors are visible (Sec. (II D)). Moreover, after having summarized the design of the flower constellation of mirrors in anti-heliotropic orbits in Sec. (II E), attitude control and the shape of the reflector are discussed in Sec. (II F). Finally, Sec. (III) investigates the power delivered to each solar farm and, furthermore, a detailed description of the loss factors is reported in Sec. (III A).

II. Orbit Design

A. Flower Constellation

The Flower Constellation (FC) takes its name from its shape as seen in the Earth rotating reference frame (ECEF). The parameters that describes a FC are the number of petals (N_p), the number of sidereal days to repeat the ground track (N_d), the number of satellites (N_s) and four other parameters that determine the phasing of the constellation: the node identification, the phasing step, and finally the RAAN (right ascension of the ascending node) (Ω) and the mean anomaly (M) of the constellation [11]. The other orbital parameters (argument of perigee (ω), inclination (i), semi-major axis (a) and eccentricity (e)) should be the same for all mirrors. However, for the purposes of this paper, the anti-heliotropic condition needs to be maintained for each mirror of the constellation and, for this reason, the orbits are slightly different from each other. This modification will allow the apsidal motion of the orbit to be synchronized with the mean apparent motion of the Sun exploiting SRP and J_2 perturbations.

The FCs are characterized by an axis of symmetry that can be arbitrarily oriented. In general, when the FC's axis of symmetry is aligned with the Earth's spin axis and the orbits are equatorial the mirror shows identical repeat ground tracks [12]. The condition to satisfy in order to achieve a

repeat ground track is given by:

$$T_r = N_p T_a = N_d T_G \tag{1}$$

where T_r is the period of repetition, T_G is the Greenwich nodal period and T_a is the anomalistic period, i.e. the time necessary to complete one petal of the flower constellation. In order to obtain a repeating orbit T_a has to satisfy the relationship in Eq. (1) and, thereafter, the semi-major axis can be evaluated from this. The design process of a specific FC starts with the choice of the parameters to describe the constellation, the generation of a complete FC and then the selective elimination of those satellites (mirrors in this case) unnecessary for the final purpose of the mission. The objective is to provide each day additional solar energy for 3 large-scale solar farms near the equator. Therefore, as for the "Sistema Quadrifoglio" [10], the parameters of the suitable FC are set as follow: $N_p = 3$, $N_d = 1$ and $N_s = 4$. Then, through Eq. (1), the anomalistic period has to be exactly 8 hours and a semi-major axis of 20270.4 km follows. The areas considered are situated in Central Africa, the Pacific coast and Oceania. In order to track these three areas, the phasing rules of the constellation of 4 mirrors are chosen so that RAAN and mean anomaly are given by:

$$\Omega = [0 \quad 90 \quad 180 \quad 270]^\circ \qquad M = [0 \quad 90 \quad 180 \quad 270]^\circ \tag{2}$$

The last parameter required to complete the design of the constellation is the orbit eccentricity. The mirrors are high area-to-mass ratio objects and so the effects of SRP (and also J_2 perturbations) would make the mirrors largely deviate from a classical Keplerian trajectory. In the next section the effect of these perturbations on the orbits is quantified and, in particular, the perturbations are exploited to estimate a suitable eccentricity to achieve a Sun-synchronous condition.

The complete flower constellation as described above would provide a $24h$-coverage of the areas of interest. However, for the purposes of this paper, only the mirrors orbiting over the regions in the night side are required. For this reason, the orbital parameters of each mirror are evaluated and "night" and "day" mirrors are defined. RAAN and mean anomaly determine the position of the orbit with respect to the Sun while the eccentricity only regulates the shape of the orbit. Therefore, it is already possible to make some distinctions between the four orbits of the mirrors: considering the position of the Sun with respect to the mirrors of the flower constellation, there are two, termed

"day" mirrors, whose apogee is always in sunlight and another two that are at the apogee when it is dark, termed "night" mirrors. Figure 1 shows the complete flower constellation in the Earth-Centred Inertial (ECI) reference frame when a nominal eccentricity of 0.5 is chosen. In particular, the continuous lines represent the orbits of the day mirrors while the dashed lines represent orbits followed by the night mirrors.

Thus, the day mirrors are now removed from the constellation and only the night mirrors will be further investigated. In particular, the incomplete flower constellation entails two mirrors with $\Omega = [0^\circ \;\; 270^\circ]$ and $M = [0^\circ \;\; 270^\circ]$.

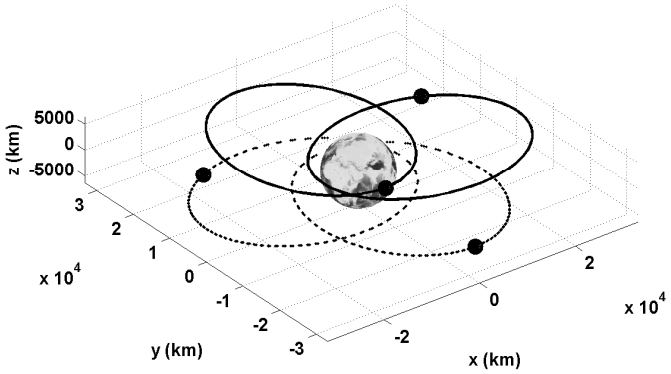

Fig. 1: Complete flower constellation with eccentricity 0.5 in the Earth's central inertial frame (ECI).

B. Anti-heliotropic Orbits

Large space mirrors are high area-to-mass ratio objects so that SRP perturbations are no longer negligible [9]. These perturbations can be exploited to generate new families of highly perturbed non-Keplerian orbits [9, 13]. Specifically, in [9], a simplified planar model of the dynamics is investigated through the Hamiltonian of the system and novel families of equilibrium in-plane orbits are identified: heliotropic and anti-heliotropic orbits, where, choosing suitable combinations of semi-major axis and eccentricity, a Sun-synchronous condition is achieved passively and the other in-plane orbital elements are constant. The former are Sun-pointing apogee orbits and entail that the mirror would be in sunlight while near the apogee. The second family of orbits generated from this analysis are Sun-pointing perigee orbits. In this case, the mirror would spend most time over the night side of

the Earth. Since the goal is to provide additional solar energy during the night or early morning and evening hours, the second family of orbits are of most interest. With respect to the analysis of the planar model investigated in [9], in this paper, the eclipse effect and the SRP perturbation due to the steering of the mirror to track the solar farm are considered during the investigation of the orbital elements through the Lagrange equations.

The orbits considered have zero inclination and for ease of illustration the ecliptic obliquity is neglected so that it is necessary to investigate only the in-plane motion. Moreover, as in [14], the normal to the surface of the mirror is assumed to be within the ecliptic plane so that SRP perturbs only the in-plane motion. With these conditions, as in [14], only three osculating orbital elements are required in order to describe the resulting trajectory, which can be expressed through the Lagrange equations [14]:

$$\frac{da}{df} = \frac{2p|r|^2}{(\mu(1-e^2))^2}\left[e\ sin(f)R + \frac{p}{|r|}T\right] \tag{3}$$

$$\frac{de}{df} = \frac{|r|^2}{\mu}\left[sin(f)R + \left(1+\frac{|r|}{p}\right)cos(f)e\ \frac{|r|}{p}T\right] \tag{4}$$

$$\frac{d\omega}{df} = \frac{|r|^2}{\mu e}\left[-cos(f)R + \left(1+\frac{|r|}{p}\right)sin(f)T\right] \tag{5}$$

where R and T are the radial and transverse components of the perturbations which the mirror is subject to given by $R = a_{J_2} + a_{SRP_R}$ and $T = a_{SRP_T}$, where a_{SRP_R} and a_{SRP_T} are given by the acceleration due to SRP along the radial and transversal direction, respectively. Differently from [9], in this work the J_2 perturbation experienced by the mirror is also considered and can be written as follow [15]:

$$a_{J_2} = \frac{3}{2}\frac{\mu}{|r|^4}R_e^2\ J_2 \tag{6}$$

where R_e is the Earth's radius and J_2 is the oblateness parameter (1.083×10^{-3}). Since the mirror needs to steer in order to track the solar farm while visible, its relative orientation with respect to the Sun is one-day periodic, but will change along the orbit. As a consequence, the SRP perturbation varies according to the steering law used, as will be considered later.

Moreover, from the theory of the umbra cone [16], the true anomalies identifying the beginning and end of the eclipse can be determined through geometrical considerations. Considering the

umbral geometry described in Fig. 2, it is possible to compute the vector $\boldsymbol{\delta}$, i.e. the vector originating at the umbral cone axis, pointing to the spacecraft at the projected spacecraft location, at time t. The true anomalies identifying the eclipse are those that satisfy the following condition:

$$|\boldsymbol{\delta}(f)| = \xi(f) \tag{7}$$

where ξ is the distance between the umbral cone axis and the umbra terminator point at the projected spacecraft location and is given by:

$$\xi = (\chi_u - |\mathbf{r_s}|)\, tan(\gamma) \tag{8}$$

In Eq. (8), χ_u is the distance between the umbral cone apex (γ) and the centre of the Earth and, as can be seen in Fig. 2, $|\mathbf{r_s}|$ is the projection of the position vector of the mirror on Earth-Sun line in ECI coordinates on the unit solar vector ($\hat{\mathbf{s}}$). Thus, when $\mathbf{r} \cdot \hat{\mathbf{s}} < 0$ and Eq. (7) is satisfied, the times as well as the true anomalies ($f_{ecl_{1,2}}$) of the beginning and ending of the eclipse are found.

In order to take the eclipse duration into account, the piecewise integrals of the three orbital parameters in Eqs. (3-5) averaged over one orbital period are considered.

In the next sections, two steering laws are investigated: a simple Earth-pointing steering law and a solar-farm-tracking steering law. The Earth-pointing steering law can be obtained analytically for illustration, whereas a numerical investigation is performed to obtain the second steering law. The steering law of the mirror is then used to estimate the SRP perturbation along the orbit and the consequential variation of the orbital parameters through Eqs. (3-5).

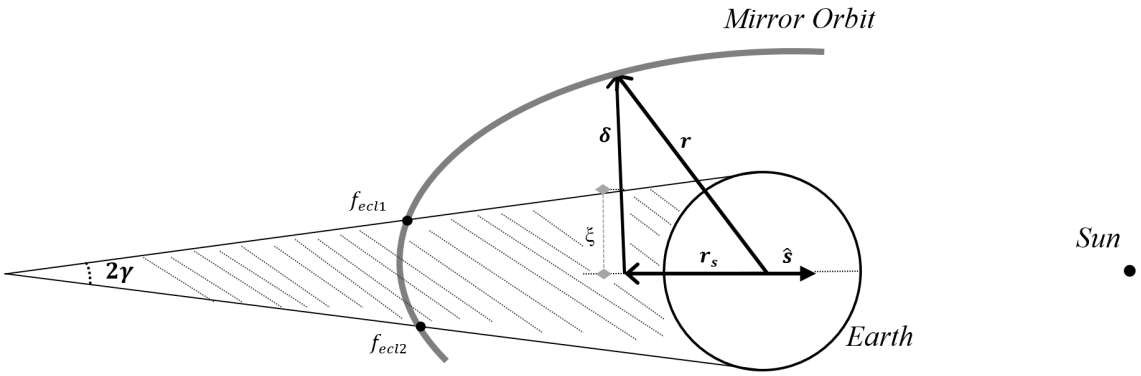

Fig. 2: Geometry of the umbral cone caused by the Earth on the orbit of the mirror.

C. First Steering Law: Earth-Centre Pointing

The first steering law investigated is an Earth-centre pointing strategy, i.e. the mirror points always towards the centre of the Earth. This can be used to estimate the impact of SRP perturbation analytically. Considering [14], where a Moon-centre pointing strategy is developed, the incident angle α (angle between the incoming and reflected solar radiation (see Fig. 4)) can be written as a function of the true anomaly f as follows:

$$\alpha = \pi - f \tag{9}$$

Thus, the acceleration perturbation due to solar radiation pressure along the radial and transversal direction can be written as [14]:

$$\mathbf{a}_{SRP}(f) = \begin{bmatrix} a_{SRP_R} \\ \\ a_{SRP_T} \end{bmatrix} = P_{SRP}\ C_r \frac{A_M}{m} sin^2\left(\frac{f}{2}\right) \begin{bmatrix} sin\left(\frac{f}{2}\right) \\ \\ cos\left(\frac{f}{2}\right) \end{bmatrix} \tag{10}$$

where P_{SRP} is the solar pressure at 1 AU equal to $4.56 \times 10^{-6}\ N/m^2$ [9], C_r is the reflectivity coefficient given by $1 + r_{sp}$ where r_{sp} is the reflectivity of the material set to 0.92 (generally aluminium) [17]. Considering Eq. (6) and Eq. (10) in Eqs. (3-5), the piecewise integrals can be written as:

$$\Delta a = \int_0^{f_{ecl_1}} \frac{da}{df} df + \int_{f_{ecl_1}}^{f_{ecl_2}} \frac{da_{SRP=0}}{df} df + \int_{f_{ecl_2}}^{2\pi} \frac{da}{df} df \tag{11}$$

$$\Delta e = \int_0^{f_{ecl_1}} \frac{de}{df} df + \int_{f_{ecl_1}}^{f_{ecl_2}} \frac{de_{SRP=0}}{df} df + \int_{f_{ecl_2}}^{2\pi} \frac{de}{df} df \tag{12}$$

$$\Delta \omega = \int_0^{f_{ecl_1}} \frac{d\omega}{df} df + \int_{f_{ecl_1}}^{f_{ecl_2}} \frac{d\omega_{SRP=0}}{df} df + \int_{f_{ecl_2}}^{2\pi} \frac{d\omega}{df} df \tag{13}$$

Here $a_{SRP=0}$, $e_{SRP=0}$ and $\omega_{SRP=0}$ in Eqs. (11-13) are the perturbations of a, e and ω due only to the Earth's oblateness since there is no SRP perturbation while the mirror is in eclipse. Every mirror completes 3 revolutions each day during which it experiences from 20 up to 58 minutes of eclipse every orbit (depending on the mirror and its orbital parameters). In this case, for the first steering law, the perturbations are identical during every revolution and Eqs. (11-13) are always valid. Therefore, the overall variation of the orbital parameters averaged over one day (T_G is the Greenwich nodal period) can be written as:

$$\Delta a_{day} = \frac{3\Delta a}{T_G} \tag{14}$$

$$\Delta e_{day} = \frac{3\Delta e}{T_G} \tag{15}$$

$$\Delta \omega_{day} = \frac{3\Delta \omega}{T_G} \tag{16}$$

Thus, substituting Eqs. (11-13) in Eqs. (14-16), the daily variation of semi-major axis, eccentricity and argument of perigee can be estimated for the orbits of the space mirrors. As expected, due to symmetry it is found that Δa_{day} and Δe_{day} are equal to zero, therefore, the one-day averaged J_2 and SRP perturbations do not affect the semi-major axis and the eccentricity of the orbit even when the eclipse is considered. A similar problem was already investigated without the J_2 perturbation in [14], however the same result is expected because of the periodicity of the J_2 perturbation along the orbit.

Moreover, $\Delta \omega_{day}$ is developed from Eq. (16) and, as expected, the summation is different from zero. SRP and J_2 perturbations therefore generate a precession of the argument of perigee. This effect can be exploited to estimate the required eccentricity of the orbit so that a Sun-following condition is achieved. The condition considered to obtain the eccentricity of the orbit is given by the requirement $\Delta \omega_{day} = \dot{\lambda_s}$. This condition is required to precess the orbit's apse line at the same rate as the Sun ($\dot{\lambda_s} = 0.9856°/day$) [18]. Through this procedure, the required eccentricity to achieve a frozen orbit is estimated to be $0.53 - 0.54$ for a mirror with an area-to-mass ratio of $30\ m^2/kg$.

This result can be verified considering the Hamiltonian system formed by the two-body dynamics of a spacecraft perturbed by J_2 and the effect of solar radiation pressure. As in [9], the system can be employed to identify families of equilibrium orbits in-plane and so the eccentricity-ϕ phase space in Fig. (3) can be obtained, where ϕ is the angle between the Sun-Earth line and the orbit apse-line. The eccentricity has an upper limit defined as $e_{max} = 1 - \frac{R_e+1000}{a}$ (indicated by the grey line in Fig. (3)) in order to avoid perigee heights below 1000 km where air drag would dominate. As it can be seen, there is only one feasible equilibrium point for $e < e_{max}$ at $\phi = \pi$ and corresponds to $e = 0.54$. All librational behaviours around $\phi = \pi$ correspond to antiheliotropic orbits [9].

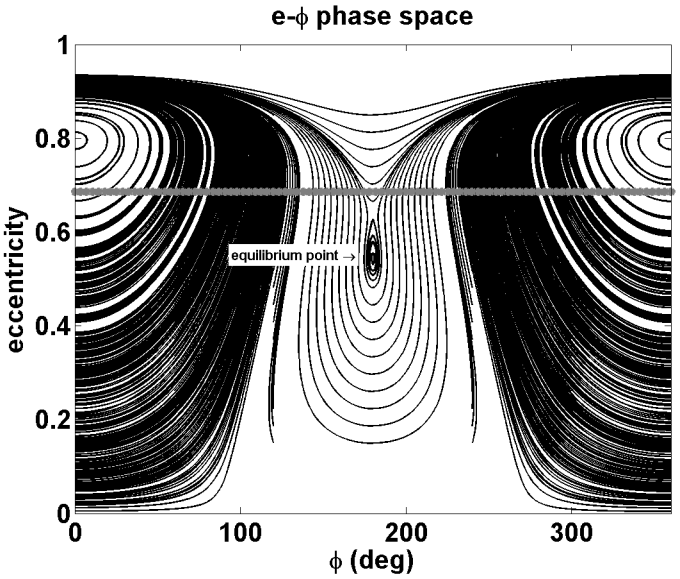

Fig. 3: Eccentricity-ϕ phase space for a mirror following an Earth-centre pointing steering law (area-to-mass ratio=30 m^2/kg, $a = 20270.4\ km$). The grey line represents the upper limit for the eccentricity.

D. Second Steering Law: Tracking of Solar Plants

With respect to the Earth-centre pointing strategy, the second steering law is more specific. Every time the mirror is near the orbit apogee and in visibility for one of the solar farms, it will steer to track it. Contrary to the first steering law described in Sec. (II C), in this case a different steering law and required orbit eccentricity is estimated for each mirror in order to achieve the Sun-following condition. For this reason, it is expected that the area-to-mass ratio of the mirror could vary from the value estimated for the first steering law.

It is important to highlight that the control laws for the mirrors need to maintain symmetry along the orbit so that the averaged variation of semi-major axis and eccentricity due to the perturbations (Eqs. (14-15)) is still zero. In order to achieve symmetry, the position of the solar farm needs to be exactly under the apogee of the orbit. The selected locations for the three solar power farms are summarized in Table (2). It is necessary that the solar farms are equidistant from each other in order to assure that the surplus solar energy is received during the night. For this reason two of the locations considered are necessarily in the ocean. Despite this, it may be actually convenient that this technology is developed outside urban areas in order to minimize the effects of nighttime

Table 2: Location of the chosen solar power farms.

	Pacific Coast	Central Africa	Oceania
longitude	90 W	30 E	151 E
latitude	0	0	0
local time	$GMT - 6h$	$GMT + 1h$	$GMT + 8h$

illumination. Also, Japan has already considered this possibility in order to overcome the problem of space unavailability on land [20]. Moreover, if a specific area that is not exactly on the equator needs to be targeted, inclined orbits should be taken into account and three-dimensional dynamics considered.

As reported also in Tab. 1, the values of RAAN and mean anomaly employed are those found previously for the night-mirrors, also, the initial argument of perigee of the orbits (ω) is set to 270°. Also, for this strategy, an area-to-mass ratio of 50 m^2/kg ($\sigma_s = 20\ g/m^2$) is considered. In order to provide this value of area-to-mass ratio the space mirror needs to be 25% lighter than the L' Garde Sunjammer solar sail [19]. Sunjammer has a sail loading of 26.6 g/m^2 (σ_s), however a mass density of 20 g/m^2 is required to achieve the range of eccentricities of interest and, therefore, the Sun-following condition. It is expected that in future the performance of space mirrors and solar sails will be improved, for example by substituting conventional substrates with more advanced materials. This improvement would make the launch of ultralight space mirrors more feasible and cost effective by decreasing their weight by an order of magnitude.

During the search of the eccentricity, the geometry in Fig. 4 is used to estimate the nadir angle (η) measured at the mirror from the sub-satellite point to the target, i.e. the solar farm [21]. The minimum elevation angle (see Fig. 4) that is considered for the mirror is $\epsilon_{min} = 24°$: this value is chosen so that the assumptions made are valid, such as the value for the atmospheric transmittance being lower than 0.9 (see Sec. (III)) for very low elevation angles. Taking into account the angular Earth's rotation (angular velocity ω_e), the geographical coordinates of the solar farms are written in general as $(\lambda + \omega_e t, \phi)$, where λ is the longitude of a point on the surface of the Earth, which is displaced by the Earth's rotation. Also, in this specific case, the latitude ϕ is equal to 0. Since

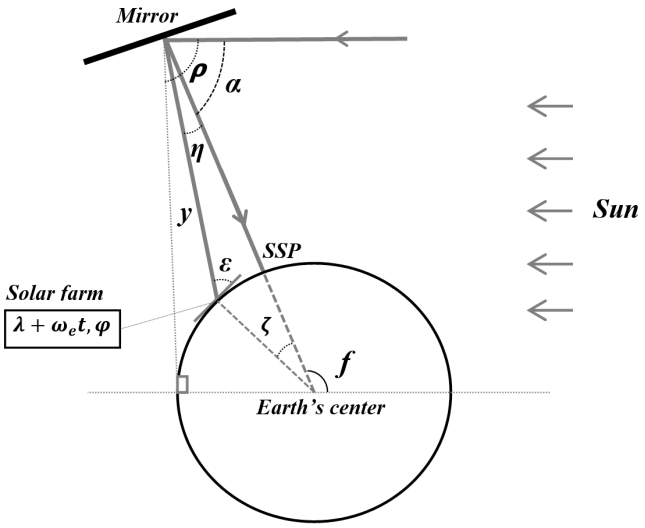

Fig. 4: Geometry of the the mirror with respect to the solar farm for the second steering law.

the position of the sub-satellite point (SSP) and the target are known, it is possible to estimate the value of the Earth central angle (ζ) and the Earth angular radius (ρ) (see [21] and Fig. 4). Then, the nadir angle is defined as follow:

$$tan(\eta) = \frac{sin(\rho)sin(\zeta)}{1 - sin(\rho)cos(\zeta)} \tag{17}$$

Once the angle η is known, similarly to the case before, the incident angle can be written as a function of the true anomaly f and η as:

$$\alpha' = \pi - f + \eta = \pi - f' \tag{18}$$

Equation (10) can still be used to compute the solar radiation pressure perturbation in this case by substituting f with $f + \eta$. The mirror steers to track the solar farms while it is visible, i.e. for elevation angles larger than ϵ_{min}. In order to maintain symmetry for the overall SRP perturbation, each mirror tracks all the three solar farms once per day. In this way the resulting eccentricities are similar.

Under these conditions, as for the previous case, the Lagrange equations are used to compute the variation of the orbital parameters. Again, Eqs. (14-15) are computed and it is found that the variation of the semi-major axis and the eccentricity are negligible since their values oscillate periodically over one day. Computing Eq. (16), it can be shown that a precession of the orbit perigee occurs. Therefore, as before, the condition $\Delta\omega_{day} = \dot{\lambda}_s T_G$ is employed to estimate the required

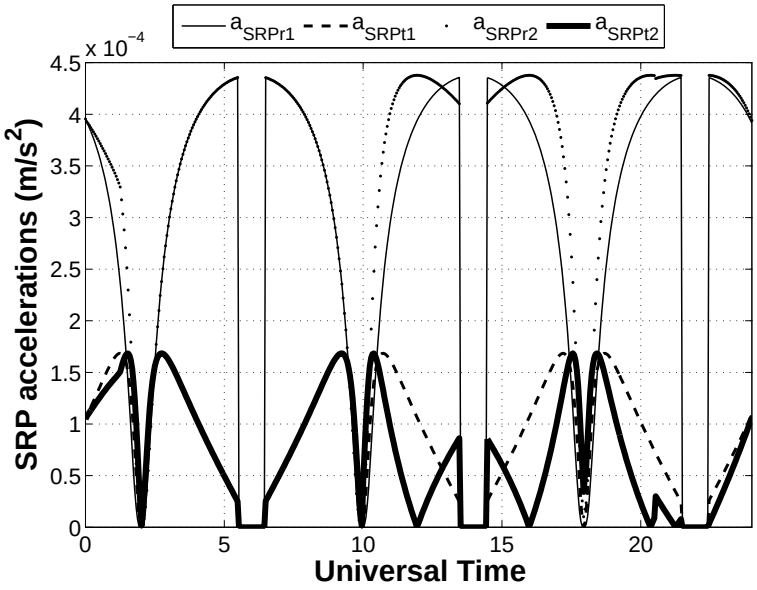

Fig. 5: Daily variation of the acceleration due to solar radiation pressure provided when the first (continuous thin line for the radial direction $\mathbf{a_{SRP_{r1}}}$, dashed line for the transversal direction $\mathbf{a_{SRP_{t1}}}$) and the second (dotted line for the radial direction $\mathbf{a_{SRP_{r2}}}$, continuous thick line for the transversal direction $\mathbf{a_{SRP_{t2}}}$) steering laws are applied.

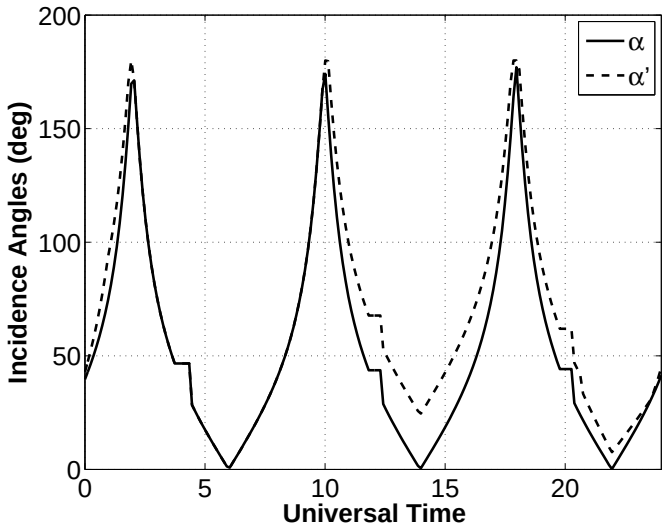

Fig. 6: Daily variation of the incidence angles for the two steering laws.

eccentricities for the orbits of the night-mirrors. The values obtained are given by $e_1 = e_2 = 0.636$. Moreover, the accelerations along the radial and transversal directions due to the solar radiation pressure for the two steering laws are reported in Fig. 5. As expected, the curves are rather similar

and sometimes there is no difference. Finally, in Fig. 6 the angles α (Earth pointing, continuous line) and α' (solar farm pointing, dashed line) are reported. Again, as expected, the curves are comparable. To track the solar farms only small attitude variations with respect to the Earth-centre pointing steering law are required.

E. Anti-heliotropic Flower Constellation for Space Reflectors

The second steering law described in the previous section allowed for an estimation of the eccentricity of the orbits exploiting J_2 and SRP perturbations and satisfying the Sun-synchronous condition. In particular the night-mirrors, i.e. those mirrors having their apogee always in the opposite direction to the Sun, are considered so that the anti-heliotropic condition is achieved.

The orbits of the night mirrors now assemble the flower constellation which can be visualized in the rotating frame in Fig. 7 and in the inertial frame in Fig. 8. The ground track and coverage [21] of the constellation can be shown in Fig. 9, where it can be seen that the mirrors orbit over the three targets of interest when they are at the apogee of each orbit. It is important to underline that the solar power farms have to be exactly below the apogee of the orbit to have symmetric SRP perturbations during the tracking of the solar farm, so that the variations of the semi-major axis and the eccentricity are zero. Considering a minimum elevation angle of 24° (see geometry

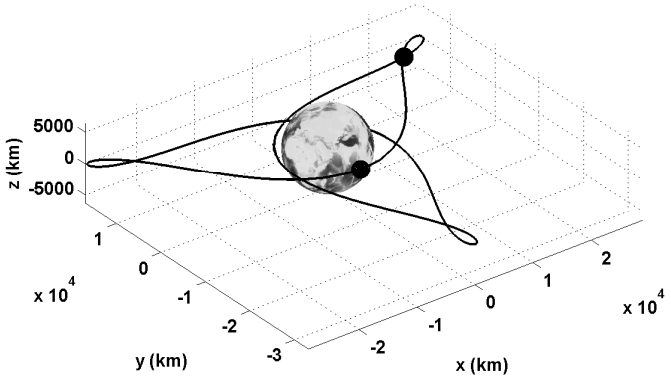

Fig. 7: Flower Constellation of the night-mirrors in the rotating Earth-centred reference frame (ECEF).

in Fig. 4), the time in visibility of each mirror over the solar farm is between 6 and 7 hours. This can be seen in Fig. 10 and 11, where the reference time is Greenwich Mean Time (GMT) and the

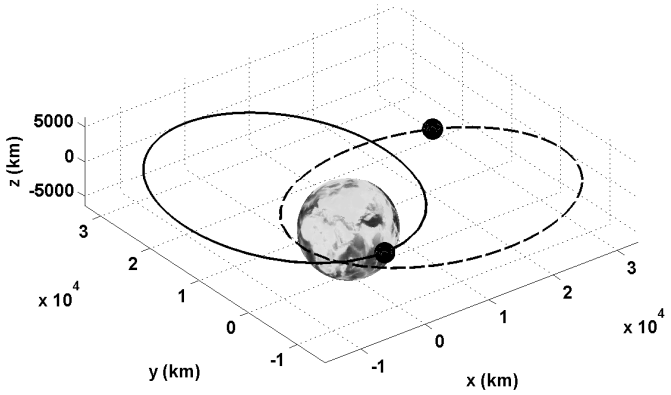

Fig. 8: Flower Constellation of the night-mirrors in the inertial Earth-centred reference frame (ECI).

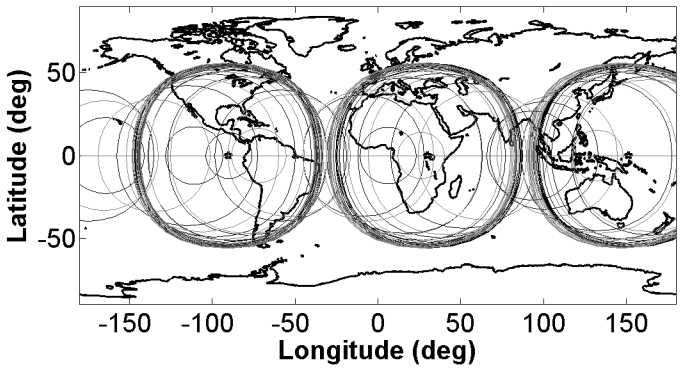

Fig. 9: Ground Track and coverage (for $\epsilon > 24°$) of the two mirrors (black line for the first mirror with $\mathbf{\Omega = 0°},\ \mathbf{M = 0°}$ and grey line for the second mirror with $\mathbf{\Omega = 270°},\ \mathbf{M = 270°}$). The locations of the solar farms are indicated by the symbol *.

time difference for each location is considered to determine the local time when the surplus energy is provided (see Table (2)). Therefore, considering the local time in the three target locations, the strategy can be summarized as follow: the first mirror ($\Omega = 0°,\ M = 0°$) tracks the first solar farm in central Africa between 1.40 AM and 8.30 AM, the second solar farm (Pacific Coast) from 2.30 AM to 9.30 AM and the third solar farm in Oceania between 00.20 AM and 7.10 AM; whereas, the

second mirror ($\Omega = 270°,\ M = 270°$) tracks the first solar farm between 7.30 PM and 2.30 AM, the second between 8.25 PM and 3.30 AM and the third solar farm from 6.20 PM to 1.30 AM. The eclipse duration for the two mirrors is approximately 20 *min* for the first mirror and 58 *min* for the second mirror and occurs during every revolution when the mirror is near apogee. It is

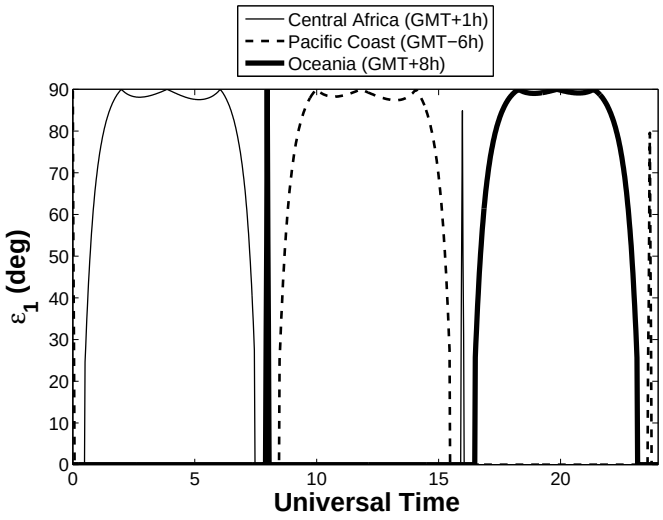

Fig. 10: Daily elevation angle of the first mirror over the three locations considered for the power farms.

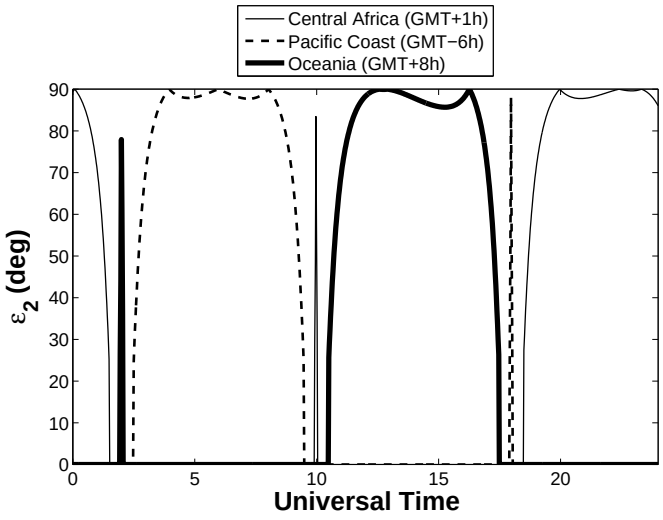

Fig. 11: Daily elevation angle of the second mirror over the three locations considered for the power farms.

interesting to highlight that in some cases the coverage also occurs during the day. Although the

Sun would clearly provide solar power anyway, this would be enhanced because the mirrors would act as concentrators of solar energy. More details on the strategy employed are reported in Table (3) which shows the time of eclipse overlapping the time of coverage, and the total coverage time is 13 h 2 min for the solar farm in Central Africa, 13 h 9 min for the Pacific coast and 12 h 47 min for the third solar farm in Oceania.

F. Attitude Control and Shape of the Reflector

As in [17], a control moment gyro (CMG) can be considered for the attitude control of the mirrors. The CMG would provide the large torque necessary to stabilize the mirrors and for the attitude control necessary to track the solar farms. Also, a low thrust propulsion system should be considered in order to periodically control the mirror attitude while the CMG is saturated and for station-keeping. This method is taken into account in [17] to control the attitude of mirrors with a diameter of 1 km. A larger space mirror can be considered a modular structure made of several 1 km-mirrors. It is important to highlight that because of the high orbit perigee considered, the effect of the atmospheric drag is completely absent.

Another interesting option is the use of electrochromic layers to effectively control the attitude of the mirror. The reflectivity of the surface would be modulated locally generating a torque that could be exploited to passively control the attitude of a large mirror. The electrochromic layers should be on the edge of the mirror in order not to affect the collection of solar power. Electrochromic coatings have been successfully employed on the IKAROS solar sail for attitude control in 2010 [22].

Finally, another important issue to deal with is the shape of the mirror. In [14], the advantages provided when a parabolic mirror is employed are shown. The area of the illuminated spot on the ground is large (of order 10^8 km^2 with a flat mirror) and, in general, the area covered by the solar farm is considerably smaller. Thus, the energy reflected outside the area of the solar farm is lost. A parabolic mirror would concentrate the reflected sunlight over a smaller area therefore reducing the loss of energy. Because of the large distance between the mirror and the solar farm, a modest mirror curvature would be required to provide the spot size required. The curvature is defined as the amount by which the surface deviates from being a flat plane and, for example, for a mirror of area 50 km^2 this is required to be only of order of magnitude 10^{-4} km^{-1}.

To obtain a parabolic mirror, a interesting option is found in [23], where the surface of a thin slack circular film is employed for an SRP shape-controlled space mirror. Although it is shown that the nominal deflection shapes due to the effect of SRP are non-parabolic, through an inverse method, the reflectivity distribution necessary to create a true parabolic deflection profile is derived analytically. The required distribution for the reflectivity could be provided through suitable coating of the film surface. However, the change in reflectivity would cause a loss in the collected solar energy that should be considered in the computation of the overall energy provided.

In order to maximize the utility of a parabolic mirror, it is necessary to adjust the focal length along the orbit so that the reflected solar radiation is always concentrated on the solar farm. Therefore, a controlled parabolic surface should be considered. It follows from the previous discussion of [23] that if the distribution of reflectivity over the surface of the mirror is controllable the focal length can be modulated. This concept could be achieved in principle through the use of electrochromic materials.

Table 3: Coverage of the solar farms during the night, evening or early morning.

# Mirror	Solar Plant	Time-Range Coverage	Eclipse Overlap	Total Coverage Time
1	Central Africa	1.28 $AM - 8.28$ AM	7 min	6h 53 min
1	Pacific Coast	2.26 $AM - 9.34$ AM	7 min	7h
1	Oceania	00.24 $AM - 7.10$ AM	9 min	6h 37 min
2	Central Africa	7.27 $PM - 2.34$ AM	58 min	6h 09 min
2	Pacific Coast	8.25 $PM - 3.32$ AM	58 min	6h 09 min
2	Oceania	6.22 $PM - 1.30$ AM	58 min	6h 10 min

III. Computation of energy delivered

In Sec. (II) the constellation design was described in detail. Two mirrors in eccentric orbits provide three locations on the ground with additional solar energy during the night or the evening hours (peak times). In this section the solar power generated from the solar farms is calculated, also taking into account the loss effect of the eclipse.

Considering the reflection of sunlight from the mirror over the Earth's surface, because of the

finite angular size of the Sun's disc, the rays reaching the mirror are not parallel and the reflected rays form an image of finite size centred about the focus [24]. The image of the Sun that is produced over the surface at a distance y (see Fig. 4) from the mirror (slant range) according to [14] can be written as:

$$A_{if}(t) = \frac{\pi}{4sin(\epsilon(t))}(D_M^2 + y^2\beta^2) \tag{19}$$

where D_M is the diameter of the flat mirror, ϵ is the elevation of the mirror above the horizon with respect to the location of the solar power farm, and β is the angle subtended by the Sun. Here β is obtained geometrically computing the ratio of the Sun's diameter over the Sun-Earth distance and is given by 0.0093 rad [6]. However, as in [14], it can be shown that if a parabolic mirror is considered better performance is achieved. The Sun's image projected over the Earth's surface by a parabolic mirror can be written as:

$$A_{ip}(t) = \frac{\pi}{4sin(\epsilon(t))}y^2\beta^2 \tag{20}$$

where in this case y is also the focal length. As noted in Sec. (II F), the parabolic mirror is assumed to be made of electrochromic materials that modify the reflectivity distribution over the surface of the mirror and make small changes to the focal length as required. In particular, considering for example a mirror of 50 km^2, a change of curvature of 6.7 10^{-5} km^{-1} would be necessary (equivalent to a change of 27 cm in the maximum height of the parabola).

Therefore, since the change of curvature of the mirrors along the orbit is so modest, the control required is small but accurate sensors and actuators need to be provided. Nevertheless, it is important to highlight that the required precision of the actuators is not key for this application (as for space telescopes), since it is only required to project the reflected light onto a coarse spot and reduce losses.

Moreover, despite the large slant range, for the geometry considered diffraction limited optics is not an issue. It is estimated that the angular resolution of the mirrors is approximately 1.57×10^{-5} $arcsec$.

Thus, accounting for all significant losses as in [17], the total power P_M delivered by the mirror

can be written as follow:

$$P_M = f_c r_{sp} \tau \psi I_0 \frac{A_M}{A_{if,ip}} cos\left(\frac{\alpha}{2}\right) \tag{21}$$

where f_c is the flatness coefficient of the reflecting surface, r_{sp} is the reflectivity coefficient already used in Sec. (II C), τ is the atmospheric trasmissivity, ψ is the cloud coefficient and $\frac{\alpha}{2}$ is the angle of incidence that describes the geometry between Sun and mirror (see Fig. 4). Also, I_0 is the solar constant given by 1.37 $\frac{GW}{km^2}$ [5]. The power received at the ground depends on the dimensions of the solar farm. If the solar farm is as large as the illuminated spot (see Eq. (20) for a parabolic mirror), the maximum power achievable would be received. Therefore, assuming a perfect pointing mirror, the power received at the ground is given by the product of the power reflected by the mirror and the area of the solar farm (A_{SF}). If the losses due to the solar farm PV array modules (ϵ_{PV}) and the ground coverage ratio (ϵ_{GCR}) are considered (to be defined later), the total power provided to each solar farm is given by:

$$P_{SF} = P_M \ \epsilon_{PV} \ \epsilon_{GCR} \ A_{SF} \tag{22}$$

All loss factors are described in detail in the next section. Finally, the total additional energy produced (GWh) by each solar farm per day is given by:

$$E_{SF} = \int_0^{T_G} P_{SF} \ dt \tag{23}$$

where $T_G = 24 \ h$.

A. Loss Factors

As noted in the previous section, losses have to be considered to estimate the energy collected by the solar farm. Some losses are due to the quality of the mirror and the efficiency of the solar farm and others are associated with environmental conditions. The mirror flatness (f_c) indicates the presence of wrinkles on the surface of the mirror. In particular, deep wrinkles with steep slopes disperse sunlight away from the illuminated spot, otherwise, shallower wrinkles disperse only some light off the target. The overall light impinging upon the illuminated spot may then be dispersed unevenly. For this reason, as well as for manufacturing purposes, the use of multiple smaller mirrors to build a large reflecting surface is advised in order to average out dispersions from wrinkles.

The root-mean-square (RMS) edge gradient of the surface of the membrane is estimated to be approximately $\sigma = 0.0002\ rad$ [17]. According to [17], the linear dispersion of the image (d_{im}) resulting from imperfections of the membrane can be computed through Eq. (24) as:

$$d_{im} = 2\sigma y \tag{24}$$

where y is the slant range. Considering Eq. (24), the illuminated spot on the ground (with diameter D_i) with the additional spill-over area caused by the dispersion is given by:

$$A_{itot} = \pi \left(\frac{D_i + d_{im}}{2} \right)^2 \tag{25}$$

Thus the flatness coefficient, indicating the loss in intensity due to surface wrinkles, can be written as:

$$f_c = \frac{A_{itot}}{A_{if,ip}} \tag{26}$$

Assuming, for example, a large mirror of diameter 8 km (approximately $A_M = 50\ km^2$), the area of the illuminated spot over the solar farm in central Africa, for example, is 5164 km^2, and the average spill-over area due to the dispersion is 1.34 km^2; therefore the illuminated area is 5336 km^2 including the spill-over area. With these conditions, the value of f_c is 88%. The mirror reflectivity

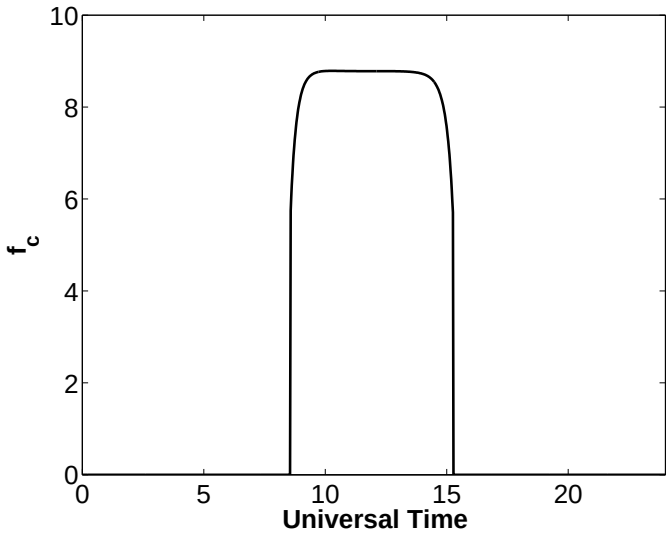

Fig. 12: Loss factor due to the surface wrinkles of the mirrors.

coefficient (r_{sp}) indicates the fraction of sunlight that is specularly reflected, therefore excluding

scattered and absorbed light. This coefficient strictly depends on the material deposited on the substrate of the mirror to provide reflectivity. If the mirror is manufactured in space, it would be possible to consider sodium for the reflective layer that would provide a reflectivity coefficient of 0.99 [17]. However, limited knowledge of the behaviour of sodium mirrors for long-term operations is available. Therefore, it would be of interest to design a test mission involving a small sodium mirror, for example on the International Space Station (ISS). Because of the present lack of information about sodium as well as its instability in the atmosphere, other materials such as silver or aluminium are considered for this task, with reflectivity coefficients of 0.98 and 0.92, respectively. The material commonly considered for this purpose is aluminium, mainly because it is inexpensive, lightweight and durable.

With regard to the solar farm, currently, the efficiency of a solar cell (ϵ_{PV}) made of silicon is approximately 20%; however, with multi-junction solar cells based on more expensive materials such as gallium arsenide or indium selenide, the overall efficiency can be as high as 31.3% (the Fraunhofer Institute for Solar Energy Systems (ISE) achieved 31.3 percent efficiency with silicon-based multi-junction solar cell (2017)). This can be further increased up to 35% (46% in laboratory conditions) [25] when concentrating optics are employed through Concentrator Photovoltaics (CPV) [26]: these systems use lenses and curved mirrors to focus sunlight onto small highly-efficient multi-junction solar cells. In this study ϵ_{PV} is set to 40%, since a future large-scale solar farm is envisaged.

Finally, the coverage ratio efficiency (ϵ_{GCR}) indicates how much of the overall area of the solar farm is actually covered with solar panels (area of the PV modules divided by the overall area of the solar farm). Generally, solar panels are tilted depending on latitude in order to maximize the amount of energy received. As the tilt angle increases, GDR must decrease to prevent reductions in energy capture due to shading. Again, the equatorial regions are the most advantageous locations because a larger tilting angle is required for solar farms at high latitudes and a minimum tilt angle is used close to the equator. Therefore, ϵ_{GCR} is set to 80% in this analysis.

Included in the losses are also the atmospheric transmittance (τ) and coefficient due to cloud coverage (ψ). The transmittance factor of reflected light travelling through the atmosphere between

the mirror and the solar farm is given, according to [27], as:

$$\tau = 0.1283 + 0.7559e^{-0.3878\ sec\left(\frac{\pi}{2}-\epsilon\right)} \tag{27}$$

where ϵ is the elevation angle measured at the solar farm location (see Fig. 4). Computing Eq. (27) for both mirrors when they are visible from the solar farm on the ground, τ is found to be approximately 64% for both mirrors. If the coefficient of scattered transmittance is also considered (6%), the overall transmittance at sea level is $\tau = 70\%$. Finally, regarding the cloud coefficient (ψ), this depends on latitude and for the equatorial regions the cloud coverage is estimated to be approximately $50 - 60\%$ [17]. However, because of their dimension, large beams are less attenuated by clouds with respect to smaller beams of light delivered for example from low Earth orbit [17] and since, in this case, the spot beam is approximately 110 km in diameter, a cloud efficiency coefficient of 0.7 (cloud coverage 30%) is considered in this study. In the case when cloudier locations are chosen, it could be possible to spread the solar farms over the illuminated spot in order to increase the chance to have clear sky for some of them.

Therefore, considering all loss factors and Eq. (23), it can be seen that the final energy delivered depends on the dimensions of the mirrors and the size of solar farms. As can be seen in Eq. (20), the illuminated area does not depend on the dimensions of the mirrors but only on their position in space (slant range (y) and elevation angle (ϵ)) and is in the range $1 - 5 \times 10^4\ km^2$. In Table (4), the energy delivered by the three solar farms is reported for several values of the area of the mirror (A_M) and the solar farms (A_{SF}).

In particular, the first 6 rows in Table (4) show the energy delivered (GWh) by mirrors of several sizes ($1 - 100\ km^2$, $\sigma_s = 20\ g/m^2$) and solar farms between 100 and 2000 km^2. It can be noted from the table that the same amount of energy is delivered in cases K and L: doubling the size of the solar farms allows half-sized mirrors (from 100 to 50 km^2) to deliver the same amount of energy.

Considering a mirror of 50 km^2 and solar farms of 250 km^2, Fig. 13 and Fig. 15 can be obtained, showing the power delivered with the mirrors. Figures (13-15) represent the distribution of the power in GW generated by each solar farm. In particular, the surplus energy delivered by both mirrors and the eclipse duration are taken into account. The shape of the curves is due to the elliptical orbits of

Table 4: Total energy generated per day from the three solar power farms for several sizes of mirrors ($\sigma_s = 20g/m^2$) and solar farms.

#	D_M (km)	A_M (km^2)	m (T)	A_{SF} (km^2)	E_{totSF1} (GWh)	E_{totSF2} (GWh)	E_{totSF3} (GWh)
A	1.13	1	20	100	0.010	0.010	0.009
B	2.52	5	100	100	0.052	0.051	0.046
C	3.57	10	200	100	0.105	0.103	0.092
D	6.18	30	600	100	0.31	0.0.31	0.28
E	7.97	50	1000	100	0.52	0.51	0.46
F	11.28	100	2000	100	1.05	1.03	0.92
G	7.97	50	1000	200	1.05	1.03	0.92
H	7.97	50	1000	250	1.31	1.29	1.15
I	7.97	50	1000	300	1.57	1.54	1.38
J	7.97	50	1000	500	2.62	2.57	2.30
K	11.28	100	2000	500	5.23	5.15	4.60
L	7.97	50	1000	1000	5.23	5.15	4.60
M	11.28	100	2000	1000	10.46	10.30	9.20
N	11.28	100	2000	2000	20.93	20.60	18.40

the mirrors. The distance of the mirrors with respect to the solar farms changes significantly along the orbit: the power generated is lower when the mirror is at apogee. Despite that the curvature of the mirror changes so that the focal length is equal to the slant range (see previous section), still the distance y appears to be the most significant term in the computation of Eq. (23) because of the limited sizes considered for the mirror (see Tab. (4)). In order to eliminate the influence of the slant range on the energy delivered the fraction $A_M/A_{if,ip}$ in Eq. (21) should be maximized and this would require mirrors of order of magnitude $A_M = 10^3\ km^2$.

Moreover, in Fig. 13 and Fig.14 the effect of the eclipse can be noted during each revolution. In the figures, local dawn/dusk lines are reported to show the duration of the day. Data is obtained considering the annual average of the solar angle above the location [28]. As can be seen, in all three cases the first mirror provides energy for three hours after dawn. However, despite the Sun already

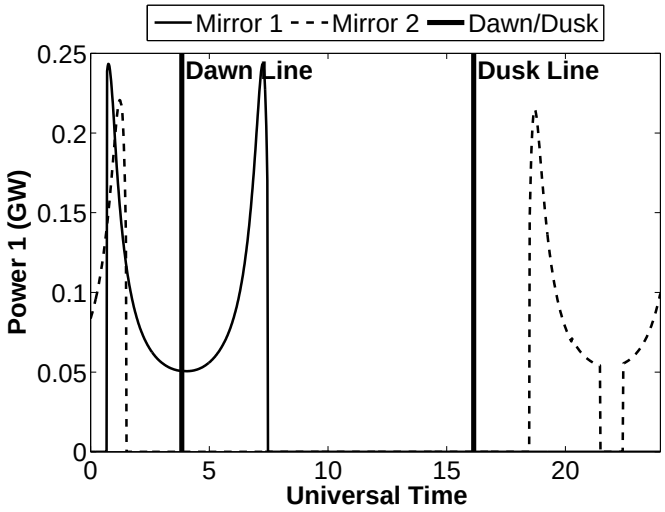

Fig. 13: Distribution of the power (GW) generated in a day by the solar farm in central Africa.

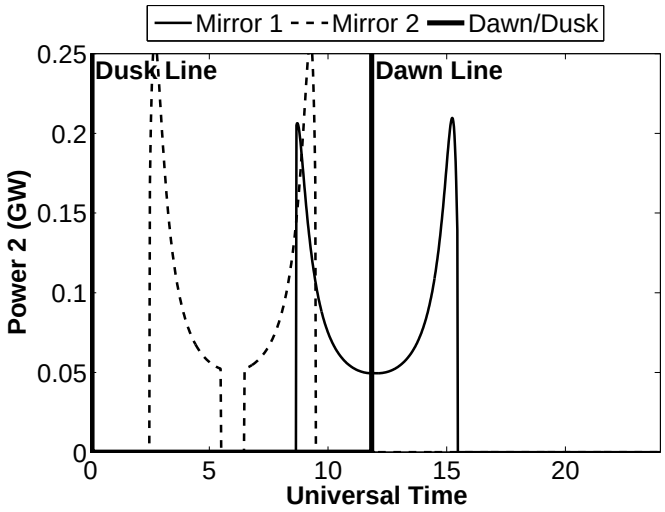

Fig. 14: Distribution of the power (GW) generated in a day by the solar farm on the Pacific Coast.

having risen, it can be demonstrated that in the first three hours after dawn, the Sun is only 20-30° (depending on the season) above the horizon; therefore, the energy supplied by the mirror is still rather advantageous for the solar farms.

It is also estimated that if a fleet of 90 constellations as those described in this paper (each consisting of two mirrors of 120 km^2) is deployed to provide energy during the hours of darkness, the price of electricity could be reduced from 9.1 cents per kWh to 6 cents per kWh.

Finally, despite that the energy delivered through the two space mirrors being as large as 20.93 GWh per day (see Table 4), the maximum flux (W/m^2) reaching the surface every day is

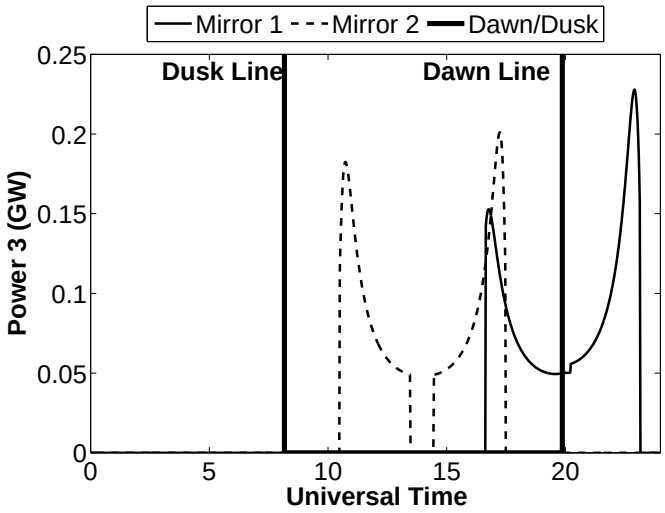

Fig. 15: Distribution of the power (GW) generated in a day by the solar farm in Oceania.

estimated to be only the 3% of normal daylight (peak intensity relative to midday Sun). This estimation is obtained considering the best case scenario where the maximum quantity of energy is received. However, given the dynamics of pricing with time of day, the energy supplied during peak hours and at dawn/dusk is of significantly greater economic value.

IV. Conclusion

A constellation of two large space mirrors (area-to-mass ratio 50 m^2/kg) is considered to provide three large-scale terrestrial solar farms (central Africa, Pacific coast, Oceania) with additional solar power during the night or peak hours. Through the concept of the flower constellation, the semi-major axis, the right ascension of the ascending node and the mean anomaly, are chosen so that the constellation has a repeat ground track and each mirror completes 3 revolutions per day. The selected mirrors spend most of their time near apogee and orbiting above the areas of interest during the night. However, the space mirrors are high area-to-mass ratio objects and, therefore, perturbations due to solar radiation pressure are important. Thus the effect of Earth oblateness and solar radiation pressure (SRP) are exploited to find suitable frozen orbits.

In this paper, two different steering laws are investigated. The first entails that the mirror points towards the centre of the Earth. Whereas the second steering law considers the track of each solar farm while the mirrors satisfy the visibility conditions. The solar farms have to be exactly

under the apogee of the orbits to assure that the perturbations due to SRP are balanced. The only parameter to be affected by SRP is the argument of the perigee. This issue is exploited to estimate the eccentricity of the orbits so that the apse line precesses at the same rate of the apparent motion of the Sun.

Considering the second steering law, each mirror orbits above the three solar farms each day. In particular, the solar farms in central Africa, Pacific coast and Oceania receive surplus energy during the night, evening or early morning for $13h$, $13h$ 09 min and $12h$ 47 min, respectively. The mirrors are in eclipse for 20 min and 58 min, respectively, during every revolution. Considering the loss factors due to the quality of the mirror, the efficiency of the solar farm and environmental conditions, the total energy generated depends on both the dimensions of the mirrors and solar farms. Considering, for example, three solar farms of 250 km^2 and two 50 km^2 parabolic mirrors, the total additional energy delivered each day is approximately 1.30 GWh for the solar farms in central Africa and on the Pacific coast and 1.15 GWh for the third farm in Oceania.

Acknowledgments

Federica Bonetti was supported by an Engineering and Physics Sciences Research Council (EPSRC) Institutional Sponsorship Grant. Colin McInnes acknowledges support from a Royal Society Wolfson Research Merit Award.

References

[1] Fraas L, Palisoc A, Derbes B. *Mirrors in dawn dusk orbit for low-cost terrestrial solar electric power in the evening.* In 51st AIAA Aerospace Sciences Meeting including the New Horizons Forum and Aerospace Exposition 2013 (p. 1191). doi:10.2514/6.2013-1191.

[2] Moore T. *Renewed interest in space solar power.* EPRI Journal. 2000 Mar 22;25(1):6-6.

[3] Tsiolkovsky K. *Plan of Space Exploration. Exploration of the Universe with Reaction Machines: Exploring the Unknown.* 1926.

[4] Ehricke KA. *The extraterrestrial imperative.* Futures. 1981 Apr 1;13(2):107-14. doi:10.1016/0016-3287(81)90018-5.

[5] Fraas LM. *Mirrors in space for low-cost terrestrial solar electric power at night.* In Photovoltaic Specialists Conference (PVSC), 2012 38^{th} IEEE 2012 Jun 3 (pp. 002862-002867). IEEE. doi: 10.1109/PVSC.2012.6318186.

[6] Potter S, Davis D. *Orbital reflectors for space solar power demonstration and use in the near term.* In AIAA SPACE 2009 Conference & Exposition 2009 (p. 6675). doi:10.2514/6.2009-6675.

[7] Turner A.E. *Formation Flying Implications of the Recoil Effects from Wireless Power Transfer.* 18^{th} AAS/AIAA Space Flight Mechanics Meeting, Galveston, TX, 27-31 January 2008, AAS 08-143.

[8] Turner A.E. *Constellation Design Considerations for Smallsats.* 27^{th} AAS/AIAA Space Flight Mechanics Meeting, San Antonio, TX, 6-9 February 2017, AAS 17-217

[9] Colombo C, Lücking C, McInnes CR. *Orbital dynamics of high area-to-mass ratio spacecraft with J_2 and solar radiation pressure for novel Earth observation and communication services.* Acta Astronautica. 2012 Dec 31;81(1):pp.137-50. doi:10.1016/j.actaastro.2012.07.009.

[10] Broglio L. *Una Politica Spaziale per il Nostro Paese, Prospettive del Progetto San Marco: Il Sistema Quadrifoglio.* Centro di Ricerca Progetto San Marco, Internal Report. 1981.

[11] Ruggieri M, Sanctis MD, Rossi T, Lucente M, Mortari D, Bruccoleri C, Salvini P, Nicolai V. *The Flower Constellation Set and its Possible Applications.* ACT Final report, Aridana. 2006 Jun;5:4108.

[12] Wilkins MP, Bruccoleri C, Mortari D. *Constellation design using flower constellations.* Paper AAS. 2004 Feb 9:04-208.

[13] Bewick R, Lücking C, Colombo C, Sanchez JP, McInnes CR. *Heliotropic dust rings for Earth climate engineering.* Advances in Space Research. 2013 Apr 1;51(7):1132-44. doi:10.1016/j.asr.2012.10.024.

[14] Bewick R, Sanchez Cuartielles JP, McInnes C. *Use of orbiting reflectors to decrease the technological challenges of surviving the lunar night.* In 62nd International Astronautical Congress 2011 Oct 3 - A5.1.11.

[15] Walter U. *Astronautics: the physics of space flight.* John Wiley & Sons; 2012 May 22. pp. 409–430.

[16] Longo CR, Rickman SL. *Method for the calculation of spacecraft umbra and penumbra shadow terminator points.* NASA; 1995 Apr.

[17] Canady Jr JE, Allen Jr JL. *Illumination from space with orbiting solar-reflector spacecraft.* NASA Technical Paper 2065 19820025545.

[18] McInnes CR, MacDonald M, Angelopolous V, Alexander D. *GEOSAIL: Exploring the geomagnetic tail using a small solar sail.* Journal of Spacecraft and Rockets. 2001 Jul;38(4):622-9. doi:10.2514/2.3727.

[19] Barnes NC, Derbes WC, Player CJ, Diedrich BL. *Sunjammer: a solar sail demonstration.* Advances in Solar Sailing. 2014 Feb 3;1:115-26.

[20] Boyd J, Sahu, A., Yadav, N., & Sudhakar, K. (2016). *Floating photovoltaic power plant: A review.* Renewable and Sustainable Energy Reviews, Volume 66, 2016, pp. 815-824, ISSN 1364-0321, doi: 10.1016/j.rser.2016.08.051.

[21] Larson WJ, Wertz JR. *Space mission analysis and design.* Microcosm, Inc., Torrance, CA (US); 1992 Dec 31. pp. 137–171.

[22] Mori O, Shirasawa Y, Mimasu Y, Tsuda Y, Sawada H, Saiki T, Yamamoto T, Yonekura K, Hoshino H, Kawaguchi J, Funase R. *Overview of IKAROS mission.* In Advances in solar sailing 2014 (pp. 25-43). Springer Berlin Heidelberg. doi:10.1007/978-3-642-34907-2_3.

[23] Borggräfe A, Heiligers J, Ceriotti M, McInnes CR. *Shape control of slack space reflectors using modulated solar pressure.* In Proc. R. Soc. A 2015 Jul 8 (Vol. 471, No. 2179, p. 20150119). The Royal Society. doi:10.1098/rspa.2015.0119.

[24] Stine, William B., and Michael Geyer. *Power from the Sun.* Power from the sun.net, 2001. `http://www.powerfromthesun.net/index.htm`.

[25] NREL (National Renewable Energy Laboratory). *Best Research-Cell Efficiencies Chart.* URL: `https://energy.gov/sites/prod/files/2016/04/f30/efficiency_chart_0.jpg`. Apr 14, 2017.

[26] M. Khamooshi, H. Salati, F. Egelioglu, A. Hooshyar Faghiri, J. Tarabishi, and S. Babadi, *A Review of Solar Photovoltaic Concentrators.* International Journal of Photoenergy, vol. 2014, Article ID 958521, 17 pages, 2014. doi:10.1155/2014/958521.

[27] Hottel HC. *A simple model for estimating the transmittance of direct solar radiation through clear atmospheres.* Solar Energy. 1976 Jan 1;18(2):129-34. doi:10.1016/0038-092X(76)90045-1.

[28] *Archive of Surface meteorology and Solar Energy.* John M. Kusterer, NASA Langley ASDC User Services, May 2017. URL: `https://eosweb.larc.nasa.gov/cgi-bin/sse/grid.cgi`. Apr 12, 2016.

[29] Ehricke KA. *Space light: space industrial enhancement of the solar option.* Acta Astronautica. 1979 Dec 1;6(12):1515-633. doi:10.1016/0094-5765(79)90003-1.